Journal of Magnetism and Magnetic Materials 473 (2019) 517–526

Contents lists available at ScienceDirect

Journal of Magnetism and Magnetic Materials

journal homepage: www.elsevier.com/locate/jmmm

Research articles

Antioxidant polymer-modified maghemite nanoparticles

Vitalii Patsula[a], Maksym Moskvin[a], Wei Xiong Siow[b], Rafal Konefal[a], Yunn-Hwa Ma[b,c,*], Daniel Horák[a,*]

[a] Institute of Macromolecular Chemistry, Academy of Sciences of the Czech Republic, Heyrovského nám. 2, 162 06 Prague 6, Czech Republic
[b] Department of Physiology and Pharmacology & Healthy Aging Research Center, College of Medicine, Chang Gung University, Guishan, Taoyuan 33302, Taiwan, ROC
[c] Department of Neurology, Chang Gung Memorial Hospital, Kwei-Shan, Taoyuan 33305, Taiwan, ROC

ARTICLE INFO

Keywords:
Magnetic
Nanoparticles
Antioxidant
Phenolic compounds
Poly(L-lysine)

ABSTRACT

Natural antioxidants, such as epigallocatechin-3-gallate and related phenolic compounds from tea, enhance particle cell-interactions and cellular uptake. In this study, surface of superparamagnetic iron oxide nanoparticles prepared by co-precipitation of Fe chlorides was modified with silica, polyethylenimine, poly(ethylene glycol), and poly(L-lysine) to protect the iron oxide core from redox-reactions with phenols, enhance uptake by the cells, prevent the particle aggregation, or enable conjugation with several phenol-based antioxidants. To reveal the relation between the particle uptake and chemical structure of the phenolic antioxidants, five of them were selected, namely phenol, phloroglucinol, chlorogenic, gallic, and tannic acid. After incubation of the phenol-modified nanoparticles with U87MG human glioma cells, intracellular levels of the reactive oxygen species were reduced in a similar manner, as measured by flow cytometry. Colorimetric iron assay revealed a comparable level of cell-associated particles, which was mostly independent on the applied external magnetic field. The results suggest that the poly(L-lysine)-based coating is responsible for the antioxidant effects of the particles; the phenol- and poly(L-lysine)-coatings enable effective colloidal stability in aqueous media and enhance cellular internalization of the nanoparticles.

1. Introduction

Investigation of radical scavengers in autoimmune or cardiovascular diseases becomes a promising research strategy replacing treatment with antioxidants during cancer chemotherapy, ineffectiveness and/or harmfulness of which has been proven [1–3]. Traditional antioxidants, such as vitamins, find fewer applications and new classes of natural compounds are emerging, among which is one of the most promising group of polyphenolic antioxidants, namely flavonoids, possessing pro-apoptotic [4], anti-proliferative [5], and anti-angiogenesis bioactivity [6]. Moreover, some, but not all phenolic antioxidants increase cellular uptake of the nanoparticles, suggesting that antioxidant activity may not be required for the enhancement of particle internalization [7].

To perform targeted delivery of the antioxidative compounds, a vast spectrum of carriers can be chosen, among which magnetic core/shell nanoparticles are the one that can be easily separated by a magnet or viewed by magnetic resonance imaging (MRI) as a contrast agent [8,9]. Magnetic nanoparticles are mostly prepared from iron salts by their co-precipitation with an alkali. The key role is played by surface characteristics of the particles in terms of their good colloidal stability in physiological media, biocompatibility (non-toxicity), and presence of reactive groups for prospective attachment of biomolecules, such as peptides, proteins, drugs, antioxidant agents, etc. Antioxidants of phenolic nature are well-known for their complex formation with iron ions, thus their direct contact with the iron oxide core should be prevented to avoid unwanted interactions [10,11]. Coating with organic and/or inorganic polymers, that are bioinert and at the same time can specifically bind a target biomolecules, is thus of primary importance. Examples of such coatings include silica, titania, poly(ethylene glycol), poly(*N*,*N*-dimethylacrylamide), poly(*N*-vinylpyrrolidone), polyethylenimine, carbohydrates (e.g., D-mannose or dextran), and poly(amino acids) [12–15]. Excellent particle internalization by the cells was achieved with maghemite (γ-Fe_2O_3) nanoparticles coated with poly(L-lysine) (PLL) [16,17]. PLL is a polypeptide composed of L-lysine amino acids linked by peptide bonds formed with amino group at α-carbon, which provides interesting properties, such as excellent hydrophilicity, biocompatibility, and biodegradability. PLL-coated surfaces support adhesion of cells [18], nucleic acids [19], peptides [20], and enzymes [21]. Our recent study demonstrated that PLL coating of γ-Fe_2O_3 nanoparticles interacted with heparan sulfate proteoglycan on the cell

* Corresponding authors at: Department of Physiology and Pharmacology, College of Medicine, Chang Gung University, Guishan, Taoyuan 33302, Taiwan, ROC (Y.-H. Ma).
E-mail addresses: yhma@mail.cgu.edu.tw (Y.-H. Ma), horak@imc.cas.cz (D. Horák).

https://doi.org/10.1016/j.jmmm.2018.10.081
Received 5 June 2018; Received in revised form 5 September 2018; Accepted 16 October 2018
Available online 17 October 2018
0304-8853/

surface, as the first step of the particle internalization by tumor cells [17]. In addition, epigallocatechin-3-gallate (EGCG), a tea catechin, attenuated internalization of PLL-coated γ-Fe_2O_3 nanoparticles, but greatly enhanced magnetic sensitivity of particle internalization by glioma cells. Deep understanding of this phenomenon gives possibility to develop new biologically active coating agents with improved selectivity and biocompatibility.

To investigate the mechanism of enhanced cellular uptake of PLL-coated particles in the presence of EGCG, PLL was chemically modified with selected phenolic compounds. As EGCG contains eight hydroxyls, including six vicinal ones, it is interesting to determine which of them triggered the mechanism of the cellular uptake. Consequently, PLL was modified with phenols containing single hydroxyl (phenol), two vicinal hydroxyls (chlorogenic acid), three hydroxyls (phloroglucinol), three vicinal hydroxyls (gallic acid), and polyphenol with vicinal hydroxyls (tannic acid). U87MG cells were used as a model system to study the particle-cell interactions to provide important information regarding applicability of the particles as a potential carrier in theranostics. Our studies demonstrated a dominant role of PLL as the antioxidant coating in nanoparticle internalization by the glioma cells.

2. Experimental

2.1. Materials

N-hydroxysuccinimide-activated methoxypoly(ethylene glycol) (PEG-NHS; M_w = 2 kDa) was purchased from Rapp Polymere (Tuebingen, Germany). poly(L-lysine) hydrobromide (PLL; M_w = 10 kDa), branched polyethylenimine (PEI; M_w = 800 Da), 1,4-aminobenzoic acid (99%), di-*tert*-butyl dicarbonate (99%), *N*,*N*′-dicyclohexylcarbodiimide (DCC; 99%), *N*-hydroxysuccinimide (NHS), trifluoroacetic acid (99%), tetramethyl orthosilicate (TMOS; 99%), 3-(trimethoxysilyl)propyl methacrylate (TMSPMA; 98%), Folin-Ciocalteu (FC) reagent, phenol (99%), phloroglucinol (99%), chlorogenic acid (95%), tannic acid, gallic acid (98%), 2,2-diphenyl-1-picrylhydrazyl (DPPH, 95%), sodium hydroxide (98%), sodium hydride (60% dispersion in mineral oil), dimethyl sulfoxide (DMSO; 99.9%), fetal bovine serum (FBS), and the components for phosphate buffered saline (PBS) were purchased from Sigma-Aldrich (St. Louis, MO, USA) and used as received. Methanol (MeOH; (99%), ethanol for UV spectroscopy (96%), acetone (98%), 2-propanol (98%), urea, sodium nitrite, sodium hydroxide, HCl (35%), P_2O_5 (98%), $NaHCO_3$ (99%), Na_2CO_3 (99%), CH_2Cl_2 (99%), triethylamine (98%), tetrahydrofuran (THF; 99%) and 1,4-dioxane (99%) were purchased from Lach-Ner (Neratovice, Czech Republic) and used as received. Minimum essential medium (MEM) and trypsin-ethylenediaminetetraacetic acid (trypsin-EDTA) were purchased from Gibco BRL (Grand Island, NY, USA). Penicillin/streptomycin/amphotericin was purchased from Upstate Biotechnology (Lake Placid, NY, USA). Dextran-coated magnetic nanoparticles (nanomag®-D COOH; 250 nm) were purchased from Micromod Partikeltechnologie GmbH (Rostock, Germany). Chloromethyl derivative of 2′,7′-dichlorodihydrofluorescein diacetate (CM-H_2DCFDA) was purchased from Molecule Probe (Waltham, MA, USA). Triethylamine and THF were dried before use with NaOH and NaH, respectively, and distilled. Dialysis membrane (3.5 and 14 kDa) was from Spectrum Labs (Rancho Dominguez, CA, USA). All aqueous solutions were prepared from ultrapure Q-water ultrafiltered on a Milli-Q Gradient A10 apparatus (Millipore; Molsheim, France).

2.2. Preparation of phenol-modified poly(L-lysine) (PPLL)

Modification of poly(L-lysine) with phenolic compounds was done according to scheme on Fig. 1.

2.2.1. Synthesis of 4-[(tert-butoxycarbonyl)amino]benzoic acid (1)

To protect amino groups, 1,4-aminobenzoic acid (21.9 mmol) was dissolved in 1,4-dioxane (50 mL) with stirring (700 rpm). Water (25 mL), triethylamine (43.8 mmol), and di-*tert*-butyl dicarbonate (43.8 mmol) were added and the mixture was stirred at room temperature (RT) for 24 h. The reaction mixture was concentrated to 50% of initial volume using a rotary vacuum evaporator at 35 °C and 10% HCl (30 mL) was added dropwise. Obtained precipitate was filtered, washed with water three times (20 mL each), and vacuum-dried with P_2O_5 for 6 h. Resulting 4-[(*tert*-butoxycarbonyl)amino]benzoic acid was purified by recrystallization from MeOH; yield: 90%. ^{1}H NMR and ATR FTIR data, which are shown in Supplementary material (SM), agreed with earlier published results [22].

2.2.2. Synthesis of N-hydroxysuccinimido-4-[(tert-butoxycarbonyl)amino] benzoate (1a)

Compound **1** (12.7 mmol) and NHS (12.7 mmol) were dissolved in dry THF (50 mL), the mixture was cooled in an ice bath, and solution of DCC (12.7 mmol) in dry THF (15 mL) was dropwise added with stirring (700 rpm). The mixture was stirred at RT for 12 h, filtered, and THF was removed from the filtrate at 35 °C using a rotary vacuum evaporator. Finally, compound **1a** was recrystallized from CH_2Cl_2 in a dry ice bath; yield: 89%. ^{1}H NMR and ATR FTIR data, which are shown in SM, were in agreement with earlier published results [23].

2.2.3. Synthesis of poly(L-lysine)-aminobenzoate (2b)

PLL (90 mg) was dissolved in DMSO (5 mL), aqueous $NaHCO_3$ (85 μmol) solution (0.4 mL) was added, and the mixture was stirred at RT for 15 min. DMSO solution (1 mL) of **1a** (43 μmol) was added with stirring (700 rpm) for 4 h, the mixture was poured into acetone and modified poly(L-lysine) (**2a**) was precipitated, separated by filtration, and washed with acetone three times (5 mL each). To remove Boc protecting group, compound **2a** was dissolved in a mixture of water and trifluoroacetic acid (1:1 v/v, 6 mL) and the solution was stirred for 2.5 h. Finally, pH of the mixture was adjusted to 7 using Na_2CO_3, poly (L-lysine)-aminobenzoate (**2b**) solution was dialyzed against water for 48 h using 3.5 kDa membrane, and freeze-dried. ^{1}H NMR and ATR FTIR data of compounds **2a**, **b** are shown in SM.

2.2.4. Synthesis of phenol-modified poly(L-lysine) (PPLL)

Compound **2b** (20 mg) was dissolved in 4 M HCl (3 mL), while sodium nitrite (1.9 mg; 28 μmol) and urea (3 mg; 50 μmol) were dissolved in water (1 mL each) at 0 °C. Sodium nitrite solution was added to solution of **2b** at 0 °C with stirring (700 rpm), urea solution was added after 10 min, and the mixture was stirred for 5 min. Solution of phenol, phloroglucinol, chlorogenic acid, or gallic acid (35 μmol each) or tannic acid (3.5 μmol) in 4 M NaOH (2.8 mL) cooled to 0 °C was added and the mixture was stirred for 2 h. Finally, pH of the mixture was adjusted to 7 using Na_2CO_3. Phenol (I)-, chlorogenic acid (II)-, phloroglucinol (III)-, gallic acid (IV)-, or tannic acid-modified PLL (V) was dialyzed against water for 48 h using 3.5 kDa membrane and freeze-dried. ^{1}H NMR and ATR FTIR data of PPLL-I-V are shown in SM.

To analyze amount of phenols in PPLL, phenolic compound, corresponding aqueous PPLL solution or water (blank; 20 μL each), Folin-Ciocalteu reagent (100 μL), and water (1.58 mL) were mixed in separate cuvettes. After 2.5 min, saturated sodium carbonate solution (300 μL) was added with shaking, the cuvettes were left at RT for 1 h in dark, and absorbance was determined using a Specord® 250 Plus UV–Vis spectrometer (Jena, Germany) at 765 nm. Amount of phenols in PLL was determined from a calibration curve against the blank.

2.3. Magnetic particle modification

2.3.1. Coating of γ-Fe_2O_3 nanoparticles with silica and introduction of methacrylate groups

Surface modification of maghemite (γ-Fe_2O_3) nanoparticles is schematically shown on Fig. 2. Starting γ-Fe_2O_3 particles were obtained by modification of an earlier described procedure [24]. Dispersion of γ-

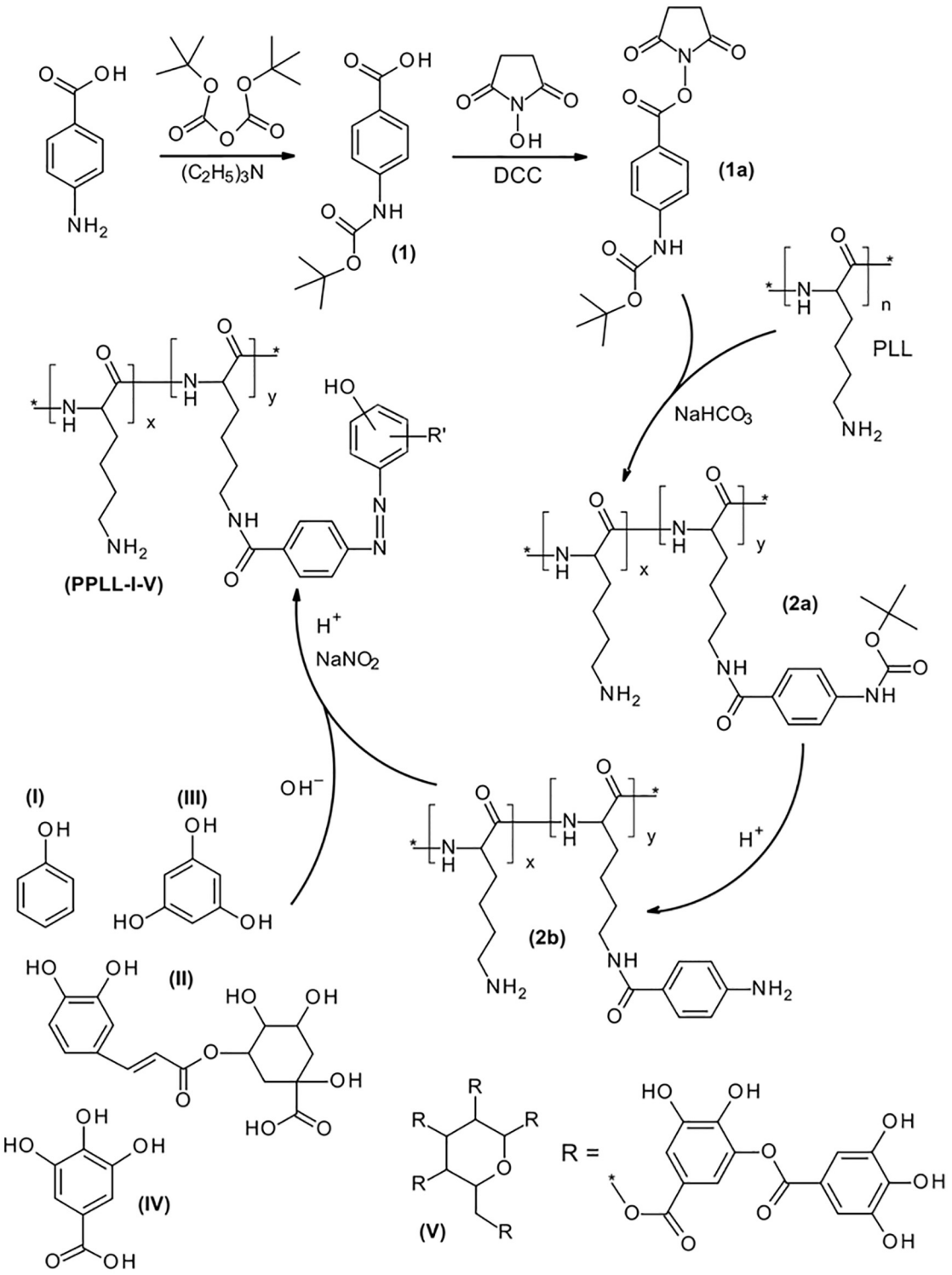

Fig. 1. Modification of poly(L-lysine) with phenolic substances. DCC – *N*,*N*′-dicyclohexylcarbodiimide; PLL – poly(L-lysine); **1** – 4-[(*tert*-butoxycarbonyl)amino] benzoic acid; **1a** – *N*-hydroxysuccinimido-4-[(*tert*-butoxycarbonyl)amino]benzoate; **2a** – 4-[(*tert*-butoxycarbonyl)amino]benzoate of poly(L-lysine); **2b** – poly(L-lysine)-aminobenzoate; PPLL-I-V – poly(L-lysine) modified with phenol, phloroglucinol, chlorogenic acid, gallic acid, and tannic acid, respectively.

Fe_2O_3 nanoparticles (350 mg) in water (10 mL) was mixed with 2-propanol (33 mL), aqueous 0.03 M NaOH (8 mL) was added, the mixture was heated to 60 °C, and TMOS (70 mg) was added with stirring (700 rpm) for 14 h. Resulting γ-Fe_2O_3@SiO_2 particles were washed with water five times (70 mL each) using magnetic separation and sonication (W-385 Heat Systems-Ultrasonics; Farmingdale, NY, USA) at 30% output and 50% duty cycle for 5 min.

γ-Fe_2O_3@SiO_2 particles were then modified with TMSPMA. The γ-Fe_2O_3@SiO_2 particles (400 mg) were dispersed in water (19 mL), 2-propanol (66 mL) and aqueous 0.03 M NaOH (15 mL) were added, the mixture was purged with argon, and TMSPMA (100 mg) was added with stirring (700 rpm) at RT for 14 h. Resulting γ-Fe_2O_3@SiO_2-MA particles were washed with water seven times (70 mL each) with magnetic separation until pH = 8.5, redispersed in water (65 mL), the

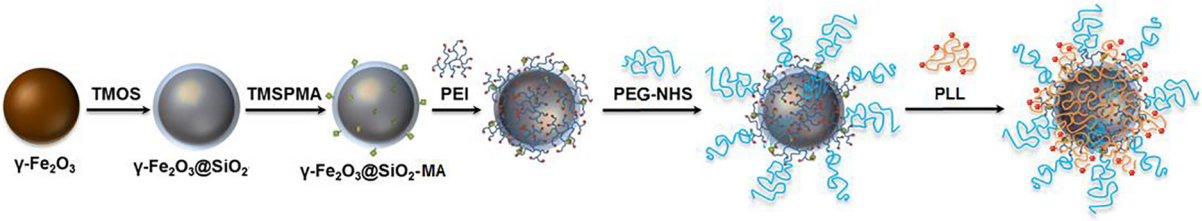

Fig. 2. Functionalization of γ-Fe_2O_3 nanoparticle surface with silica, polyethyleneimine (PEI), poly(ethylene glycol) (PEG), poly(L-lysine) (PLL), and/or phenol-modified PLL. TMOS – tetramethyl orthosilicate, TMSPMA – 3-(trimethoxysilyl)propyl methacrylate.

dispersion purged with argon, and sonicated for 5 min.

2.3.2. Coating with polyethylenimine

PEI (289 mg) was dissolved in water (4 mL), pH was adjusted to 9 by the addition of 35% HCl, and the solution was added to aqueous dispersion (19 mL) of γ-Fe_2O_3@SiO_2-MA nanoparticles (6 mg/mL) with sonication for 2 min (Hielscher UP200S ultrasonic processor; 30% power). The mixture was purged with argon for 15 min and heated to 70 °C for 18 h with stirring (700 rpm). Finally, γ-Fe_2O_3@SiO_2-PEI particles were washed with water six times (30 mL each) until pH = 7.5 and separated by centrifugation (6000 rpm).

2.3.3. Coating with PEG

Aqueous PEG-NHS (45 mg) solution (1 mL) was added to aqueous γ-Fe_2O_3@SiO_2-PEI (45 mg) dispersion (6.5 mL) with sonication for 30 s (Hielscher UP200S ultrasonic processor; 30% power) and the mixture was stirred (500 rpm) at RT for 18 h. To remove unreacted PEG, the dispersion was dialyzed against water for 48 h using 14 kDa membrane. Resulting particles were denoted as γ-Fe_2O_3@SiO_2-PEI-PEG.

2.3.4. Coating with PLL and PPLL

An aqueous PLL or PPLL solution (0.187 mg/mL; 3.21 mL) was dropwise added to a stock aqueous γ-Fe_2O_3@SiO_2-PEI-PEG dispersion (5.6 mg/mL; 11.78 mL) under sonication (Hielscher UP200S ultrasonic processor; 30% power) in an ice-cool bath. After addition of PLL or PPLL solution, the dispersion was sonicated at 0 °C for 3 min. The resulting γ-Fe_2O_3@SiO_2-PEI-PEG-PPLL-I-V colloid (shortly denoted as γ-Fe_2O_3@PPLL-I-V) had concentration 4.4 mg of particles per mL.

2.4. Characterization methods

Nanoparticles were observed in a Tecnai Spirit G^2 transmission electron microscope (TEM; FEI; Brno, Czech Republic). Number-average diameter (D_n), weight-average diameter (D_w), and dispersity ($Đ = D_w/D_n$) were calculated using Atlas software (Tescan Digital Microscopy Imaging; Brno, Czech Republic) by statistical evaluation of 300 particles from TEM micrographs. Hydrodynamic diameter (D_h) and ζ-potential were determined by dynamic light scattering (DLS) using a Nano-ZS Zetasizer ZEN3600 Model (Malvern Instruments, UK). To investigate the effect of ionic strength and pH on the ζ-potential, the particle dispersion (4.4 mg/mL; 50 µL) was diluted with aqueous NaCl solution (1 mL) of different concentrations and phosphate buffer of various pH, respectively. Relative inorganic contents were determined using a Perkin Elmer TGA 7 Thermogravimetric Analyzer (Norwalk, CT, USA). Surface-modified γ-Fe_2O_3 nanoparticles were heated in air from RT to 800 °C at 10 °C/min. ATR FTIR spectra were obtained on a Perkin-Elmer Paragon 1000PC spectrometer (Waltham, MA, USA) using a Specac MKII Golden Gate single-attenuated total reflection (ATR) system with a diamond crystal and the angle of incidence 45°.

^{1}H NMR spectra were recorded with a Bruker Avance III 600 spectrometer in deuterated DMSO with hexamethyldisiloxane internal standard (0.05 ppm). The width of 90° pulse was 10 µs, relaxation delay 10 s, acquisition time 2.18 s, 16–250 scans.

2.5. Cell culture

Human glioma cells U87MG were supplied by Food Industry Research and Development Institute (Hsinchu, Taiwan), cultured in minimal essential medium supplemented with 10% FBS and 1% penicillin/streptomycin/amphotericin at 37 °C in an incubator under 5% CO_2 atmosphere and subcultured every 3–4 days.

2.5.1. Colorimetric iron assay

U87MG cells were cultured in a 24-well culture plate until 80–90% confluence and incubated with γ-Fe_2O_3@PLL or γ-Fe_2O_3@PPLL nanoparticles (100 µg/mL) for 3 h in the absence (Mag −) or presence (Mag +) of the NdFeB magnet underneath the cells. Magnetic field was applied for 5 min after addition of nanoparticles to ensure their sedimentation [25]. The cells were then trypsinized and treated with 10% hydrochloric acid at 55 °C for 4 h, which was followed by addition of ammonium persulfate (1 mg/mL) and 1 M KSCN. The amount of iron was determined using a Victor 3 Multilabel Plate Reader (PerkinElmer; Waltham, MA, USA) at 490 nm; content of cell-associated magnetic nanoparticles was determined using a calibration curve.

2.5.2. Flow cytometry

U87MG cells were co-incubated with γ-Fe_2O_3@PLL or γ-Fe_2O_3@PPLL nanoparticles (100 µg/mL) at 37 °C for 3 h, washed twice with PBS, incubated with 6 µM CM-H_2DCFDA for 1 h, and subjected to a FACSCalibur flow cytometer (Becton Dickenson; Mississauga, CA, USA) with a 488 mm laser. Absorbance was detected at 535 nm to quantitatively analyze intracellular reactive oxygen species (ROS) signal (FL-1). The side scatter height (SSC-H) and forward scatter height (FSC-H) indicated cellular complexity and cell volume, respectively. For intracellular ROS analysis, the FL-1 signal gate was set between 5 and 6250 to exclude the background signals.

2.5.3. Cytotoxicity determination

The cytotoxicity of the particles was determined using a WST-8 assay (CCK-8 kit, Sigma-Aldrich) according to manufacturer's instruction. Briefly, U87MG cells were cultured in a 24-well plate until 80–90% confluence, followed by incubation with 100 µg/mL of particles with or without the magnet underneath. After 3 or 24 h of incubation, cells were washed with PBS twice and incubated with CCK-8-containing medium (10%) for additional 1 h. Absorbance of the supernatant from each sample was measured (VICTOR3 Multilabel Plate Reader; PerkinElmer; Waltham, MA, USA) at 450 nm to calculate percentage of viability.

3. Results and discussion

3.1. Phenol-modified PLL (PPLL)

Due to an increased electron density at aromatic ring, phenolic substances are well-known to easily undergo electrophilic substitution to covalently bind PLL via azo-coupling reaction (Fig. 1). At the beginning, 4-[(*tert*-butoxycarbonyl)amino]benzoic acid (**1**) was prepared by reaction of 1,4-aminobenzoic acid with di-*tert*-butyl dicarbonate and

converted to **1a** via coupling with NHS in the presence of DCC. Compound **1a** was then reacted with PLL and protecting *t*-Boc group was removed by treatment with trifluoroacetic acid, resulting in aromatic amine-modified PLL (**2b**). 4-Aminobenzoic acid was incorporated in PLL structure due to ability of its aromatic amino groups to form more stable diazonium ions than aliphatic amino groups of L-lysine. According to ^{1}H NMR (data not shown), degree of functionalization of PLL with aminobenzoic acid was 11 mol.%. Finally, compound **2b** was converted into PLL diazonium salt by reaction with sodium nitrite in the presence of HCl. Formed diazonium ion is a strong electrophile, easily reacting with electron-rich substrates, such as phenols. After addition of phenolic compound to the reaction mixture containing diazonium salt of PLL, the mixture changed color to yellow (phenol) or brown (all other phenolic compounds). The resulting phenol-, chlorogenic acid-, phloroglucinol-, gallic acid-, and tannic acid-containing PLLs were denoted as PPLL-I-V. The chemical structure was confirmed by ATR-FTIR and ^{1}H NMR spectroscopies. Content of phenolic compounds reached 0.24, 0.72, 1.41, 0.5, and 0.11 μmol/mg in PPLL-I-V, respectively, as determined using Folin-Ciocalteu reagent and UV–Vis spectroscopy. Various amounts of bound phenols were attributed to their different reactivity. In particular, phloroglucinol has three hydroxyls, oxygen of each provides one electron pair to benzene ring, producing more electron-rich structure than phenols with one or two hydroxyls. As a result, phloroglucinol was more reactive during electrophilic substitution than chlorogenic acid and phenol, yielding higher conversion. Gallic acid with its electron-withdrawing carboxyl group and decreased electron density in the aromatic ring exhibited also reduced reactivity during azo-coupling with compound **2b** and lower conversion compared to that of phloroglucinol. Concentration of tannic acid, which forms insoluble complexes with proteins via hydrogen bonds [26], had to be kept < 1.25 μmol/mL to avoid precipitation.

3.2. Coating of γ-Fe_2O_3 nanoparticles with silica, PEI, PEG, and PPLL

Starting superparamagnetic γ-Fe_2O_3 core nanoparticles were obtained by an aqueous co-precipitation of Fe(II) and Fe(III) chlorides with ammonia and oxidation with hydrogen peroxide [24]. Morphology, including the particle size and its distribution, were analyzed by TEM (Fig. 3A). Number-average particle diameter D_n amounted to 12 nm with a dispersity $Đ = 1.34$, characterizing moderate width of the particle size distribution. In contrast, hydrodynamic diameter D_h was 68 nm, suggesting that the nanoparticles may form weak associates in water due to magnetic attractions (Table 1).

3.2.1. γ-Fe_2O_3@SiO_2 and γ-Fe_2O_3@SiO_2-MA nanoparticles

Surface of the γ-Fe_2O_3 nanoparticles has to be protected from undesirable interactions with phenolic compounds, which can form complexes with Fe ions [27]. In this report, γ-Fe_2O_3 surface was firstly coated with biocompatible hydrophilic silica using TMOS in alkaline medium, which was followed by introduction of methacrylate groups with TMSPMA (Fig. 2); resulting particles were denoted as γ-Fe_2O_3@SiO_2-MA. Their D_n (15 nm; Table 1) was higher than that of uncoated particles, which proved the successful coating with silica. Infrared spectrum of the γ-Fe_2O_3@SiO_2-MA exhibited two peaks at 934 and 1014 cm^{-1} attributed to ν_d(Si—OH) and ν_{as}(Si—O—Si) vibrations, respectively (Fig. SM1). Bands at 1123, 1314 and 1420 cm^{-1} were assigned to ν(C—O), ν_d(C—H), and ν_d(CH_3) vibrations, respectively. Signals at 1632 and 1721 cm^{-1} corresponded to ν_{as}(C═O) and ν_s(C═O) stretching vibrations, respectively. Peaks at 2878 and 2938 cm^{-1} were attributed to ν_s(CH_2) and ν_{as}(CH_3) stretching vibrations, respectively. Broad band of O—H stretching vibrations was situated at ~3400 cm^{-1}. ATR FTIR spectra thus confirmed successful coating of γ-Fe_2O_3 nanoparticles with methacryloyl-functionalized silica. The content of organic compounds on the nanoparticle surface (3.9 wt%) was estimated using TGA (Table 1; Fig. SM2).

3.2.2. γ-Fe_2O_3@SiO_2-PEI nanoparticles

To introduce substantial amount of reactive groups on the γ-Fe_2O_3@SiO_2-MA particle surface needed for future immobilization of PEG, branched PEI containing tens of secondary amino groups per molecule was selected as a modification agent, undergoing Michael addition with electrophiles, such as methacrylates. As a result, amino groups were introduced in the nanoparticles denoted as γ-Fe_2O_3@SiO_2-PEI. Hydrodynamic size of the γ-Fe_2O_3@SiO_2-MA and γ-Fe_2O_3@SiO_2-PEI particles was similar, 149 and 152 nm, respectively, which was much more than D_h of the uncoated particles. This may be attributed to the increased hydrophilicity of the particle surface, as well as to thicker hydration layer consisting of polymer chains. However, ζ-potential of the γ-Fe_2O_3@SiO_2-MA nanoparticles in water (−65 mV) changed to 55 mV in γ-Fe_2O_3@SiO_2-PEI particles, indicating presence of positively

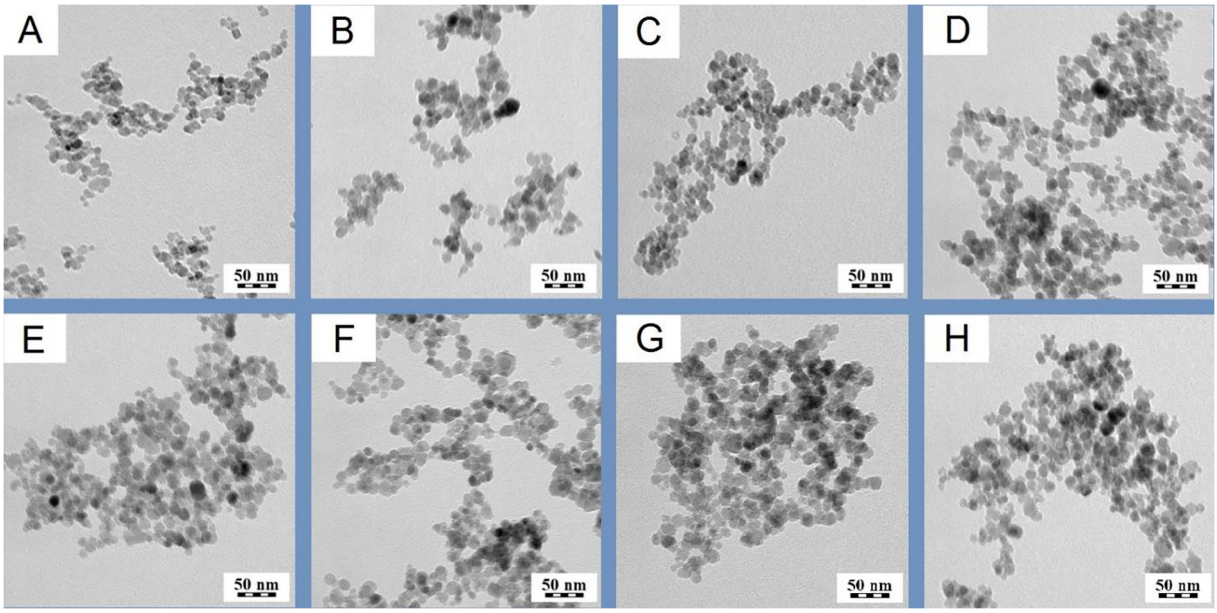

Fig. 3. TEM micrographs of (A) γ-Fe_2O_3, (B) γ-Fe_2O_3@SiO_2-PEI-PEG, (C) γ-Fe_2O_3@PLL, (D) γ-Fe_2O_3@PPLL-I, (E) γ-Fe_2O_3@PPLL-II, (F) γ-Fe_2O_3@PPLL-III, (G) γ-Fe_2O_3@PPLL-IV, and (H) γ-Fe_2O_3@PPLL-V nanoparticles.

Table 1
Characteristic properties of neat and surface-modified γ-Fe_2O_3 nanoparticles.

Particles	D_n (nm)	$Đ$	D_h[a] (nm)	ζ-potential (mV)	Coating (wt%)[b]
γ-Fe_2O_3	12	1.34	68 ± 6	42 ± 0.6	–
γ-Fe_2O_3@SiO_2-MA	15	1.28	149 ± 7.3	−65 ± 0.4	3.9
γ-Fe_2O_3@SiO_2-PEI	17	1.26	152 ± 5.5	55 ± 5.1	4.8
γ-Fe_2O_3@SiO_2-PEI-PEG	17	1.28	129 ± 7.1	34 ± 1.5	32.6

[a] In water (pH = 3.8, 9.2, 6.8, and 6.5 for γ-Fe_2O_3, γ-Fe_2O_3@SiO_2-MA, γ-Fe_2O_3@SiO_2-PEI, and γ-Fe_2O_3@SiO_2-PEI-PEG, respectively).
[b] According to thermogravimetric analysis (TGA).

charged PEI on the particle surface (Table 1). ATR FTIR spectrum of γ-Fe_2O_3@SiO_2-PEI was similar to that of γ-Fe_2O_3@SiO_2-MA particles (Fig. SM1). However, a small difference was observed due to a new peak at 1517 cm^{-1} attributed to $\nu(NH_2)$ bending vibration. In addition, a band at 1721 cm^{-1} corresponding to ν_s(C═O) stretching vibration disappeared, indicating thus covalent binding of PEI to methacrylate groups. In contrast to the TGA of γ-Fe_2O_3@SiO_2-MA, that of γ-Fe_2O_3@SiO_2-PEI particles demonstrated higher content of organic coating (4.79 wt%; Table 1; Fig. SM2). As a result, amount of bound PEI was 0.9 wt%, corresponding to 0.21 mmol of amino groups per gram of the particles.

3.2.3. γ-Fe_2O_3@SiO_2-PEI-PEG nanoparticles

To avoid aggregation of the particles, they have to provide not only electrostatic, but also steric repulsion. Amino groups of PEI were therefore reacted with PEG-NHS to covalently bind biocompatible hydrophilic PEG to the nanoparticle surface. TEM measurements revealed that the average size of PEG-coated nanoparticles did not change compared to γ-Fe_2O_3@SiO_2-PEI, however both particles were about 4 nm larger than initial maghemite cores (Fig. 3B; Table 1). According to DLS, D_h and ζ-potential of γ-Fe_2O_3@SiO_2-PEI-PEG nanoparticles decreased to 129 nm and 34 mV, respectively, compared to γ-Fe_2O_3@SiO_2-PEI particles, due to a highly hydrophilic nature of PEG providing strong steric repulsion. Consequently, γ-Fe_2O_3@SiO_2-PEI-PEG particles exhibited excellent colloidal stability in water. ATR FTIR spectrum of the γ-Fe_2O_3@SiO_2-PEI-PEG nanoparticles demonstrated a new peak at 1103 cm^{-1} attributed to ν_s(C—O—C) stretching vibrations, originating from PEG (Fig. SM1). TGA of the γ-Fe_2O_3@SiO_2-PEI-PEG particles confirmed higher content of organic compounds (32.6 wt%) compared to the γ-Fe_2O_3@SiO_2-PEI particles (Table 1, Fig. SM2). As a result, amount of PEG bound on the particle surface was estimated to 27.8 wt %.

3.2.4. γ-Fe_2O_3@PPLL nanoparticles

Finally, surface of the γ-Fe_2O_3@SiO_2-PEI-PEG nanoparticles was coated with PLL and/or PPLL. According to TEM, the particles had sizes close to that of γ-Fe_2O_3@SiO_2-PEI-PEG, with moderately broad size distributions (Fig. 3C—H; Table 2). D_h (~135 nm) and ζ-potential of all

Table 2
Characteristic properties of nanoparticles coated with neat and phenol-modified PLL.

Particles	D_n (nm)	$Đ$	D_h[a] (nm)	ζ-potential (mV)
γ-Fe_2O_3@PLL	14	1.31	134 ± 1.3	28 ± 0.4
γ-Fe_2O_3@PPLL-I	15	1.26	132 ± 2.2	29 ± 0.5
γ-Fe_2O_3@PPLL-II	16	1.22	136 ± 1.7	32 ± 2.1
γ-Fe_2O_3@PPLL-III	15	1.27	140 ± 5.2	30 ± 0.1
γ-Fe_2O_3@PPLL-IV	16	1.30	133 ± 2.2	25 ± 0.7
γ-Fe_2O_3@PPLL-V	15	1.28	125 ± 1.2	26 ± 0.3

[a] In water (pH = 6.5); PEI – polyethylenimine; PEG – poly(ethylene glycol); PLL – poly(L-lysine); PPLL-I-V – poly(L-lysine) modified with phenol, chlorogenic acid, phloroglucinol, gallic acid, and tannic acid, respectively; D_n – number-average particle diameter (TEM); $Đ$ –dispersity; D_h – hydrodynamic diameter (DLS).

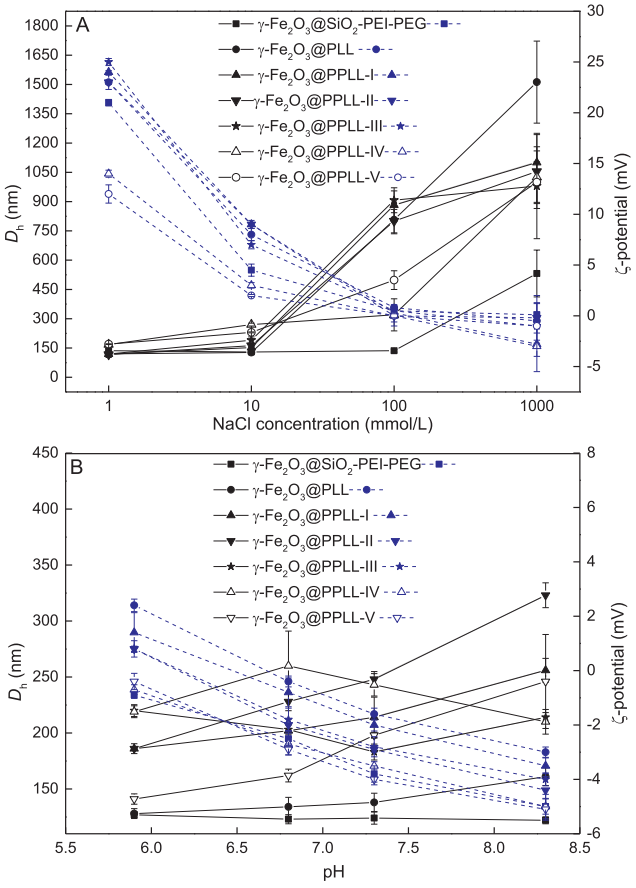

Fig. 4. Dependence of hydrodynamic diameter D_h (full line) and ζ-potential (dashed line) of γ-Fe_2O_3@SiO_2-PEI-PEG nanoparticles coated with PLL and PPLL on (A) NaCl concentration (pH = 6.5) and (B) pH (measured in 0.1 M PBS).

PLL-modified particles in water (~30 mV) were comparable to those of γ-Fe_2O_3@SiO_2-PEI-PEG nanoparticles (Table 2). Additionally, colloidal stability of the newly prepared particles was determined in water at different NaCl concentrations (10^{-3} – 1 M) and in phosphate buffer (pH 5.9–8.5) simulating physiological conditions (Fig. 4A, B). γ-Fe_2O_3@SiO_2-PEI-PEG particles were unstable only in 1 M NaCl solution, where D_h rapidly increased to 530 nm. In contrast, all types of PLL-coated nanoparticles were stable in 1 and 10 mM NaCl solutions, while the hydrodynamic size increased at higher salt concentration due to the particle aggregation (Fig. 4A). This suggests that the particles were sensitive to presence of ions in the medium due to the highly charged PLL shell on the surface. The interaction of PLL and PPLL with the particle surface is believed to occur by hydrogen bonding between carbonyls in poly(L-lysine) and amine groups on the particle surface and also by non-specific adsorption of PLL or PPLL. With increasing NaCl concentration, ζ-potential of all investigated particles decreased from ~22 mV (14 mV for γ-Fe_2O_3@PPLL-IV-V) up to −4 mV due to

compression of electrical double layer on the particle surface [28]. When the γ-Fe_2O_3@SiO_2-PEI-PEG and γ-Fe_2O_3@SiO_2-PEI-PEG-PLL (denoted as γ-Fe_2O_3@PLL) particles were investigated by DLS at various pH, their D_h remained constant in the range 130–160 nm (Fig. 4B). On the other hand, the hydrodynamic diameter of all PPLL-coated nanoparticles did not substantially change at pH 5.9–7.3, but the particles started to aggregate at pH 8.4 (D_h > 250 nm) and their ζ-potential slightly diminished from −0.4 mV (pH 5.9) to −5 mV (pH 8.4; Fig. 4B), because PLL polycation charge naturally decreased with increasing pH [29]. Moreover, DLS measurements performed at pH close to physiological conditions confirmed low negative ζ-potential of PLL-modified particles. On the other hand, the dependence of ζ-potential of γ-Fe_2O_3@PPLL-V nanoparticles on pH had slightly different trend; the highest D_h (260 nm) was observed at pH = 6.8, while it decreased with additional pH increase. We can thus hypothesize that such behavior arose from the crosslinking of individual particles by hydrogen bonds originating from complexation of tannic acid hydroxyls and amino groups of long PLL chains (M_w = 100 kDa). At alkaline pH, hydrogen bonds split and D_h of the particles decreases, which explains lower colloidal stability of the PLL-coated particles at pH > 6.5 and high NaCl concentration than that of the initial γ-Fe_2O_3@SiO_2-PEI-PEG particles, stability of which was mostly maintained by steric repulsion. Nevertheless, aqueous dispersions of γ-Fe_2O_3@PPLL-I-V particles exhibited good colloidal stability.

ATR FTIR spectra of all PLL-coated nanoparticles were similar to that of γ-Fe_2O_3@SiO_2-PEI-PEG (Fig. SM1). A new peak at 1537 cm^{-1} assigned to ν(NH) deformation vibration originated from amide bond in PLL.

3.3. Determination of ROS by flow cytometry

In order to determine antioxidant activity at the cellular level, evaluation of the nanoparticle entry and uptake is necessary. γ-Fe_2O_3@PLL and γ-Fe_2O_3@PPLL-I-V particles (100 μg/mL) were incubated with U87MG cells for 3 h. In the absence of magnetic force, content of cell-associated γ-Fe_2O_3@PLL and γ-Fe_2O_3@PPLL-I-V particles increased by 2–3 fold of that with nanomag®-D (Fig. 5). This can be explained by attraction of positively charged PLL on the particle surface to the negatively charged heparan sulfate proteoglycan on the cell membranes

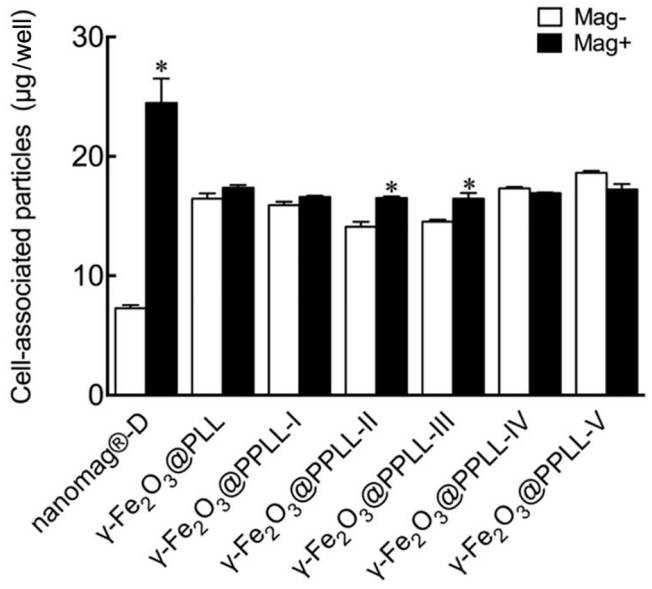

Fig. 5. Interaction of γ-Fe_2O_3@PLL and γ-Fe_2O_3@PPLL-I-V particles with U87MG cells. Magnetic field was applied for 5 min before (Mag −) or during the 3-h incubation (Mag +). Values are means ± SE (n = 3). *p < 0.05 compared with the corresponding control group.

[17], in contrast to repulsive forces between negatively charged nanomag®-D (carboxydextran-coated magnetite) and the cells. Magnetic force enhanced amount of cell-associated nanomag®-D particles by three fold, but exerted only minor or no effect on levels of cell-associated γ-Fe_2O_3@PPLL-II and γ-Fe_2O_3@PPLL-III, respectively. The results are consistent with previous findings that magnetic force did not enhance the γ-Fe_2O_3@PLL uptake by glioma cells [17]. Since the cells in the Mag-group were subjected to magnetic force for 5 min to induce sedimentation, amount of cell-associated nanomag®-D particles increased due to their enhanced cell interactions, which was in accordance with earlier reports on magnetically driven particle internalization [17] and gene delivery [30]. Moreover, the findings suggest that poly(L-lysine) chains of the γ-Fe_2O_3@PLL and γ-Fe_2O_3@PPLL particles are a key component in the nanoparticle-cell interaction. PEG is well-known to attenuate adsorption of proteins and interaction with the cells [31], decreasing thus the effect of magnetic field on association of the particles with the cells. Nevertheless, relatively low magnetically induced association of γ-Fe_2O_3@PLL and γ-Fe_2O_3@PPLL nanoparticles with the cells cannot be ascribed to steric repulsion of PEG as one of the components of the rather complex polymer shell surrounding the γ-Fe_2O_3 particle core, because magnetic insensitivity on particle internalization was also observed earlier with PEG-free γ-Fe_2O_3@PLL particles [17]. In addition, γ-Fe_2O_3@PLL and γ-Fe_2O_3@PPLL nanoparticles had small negative charge in PBS at pH > 7 (Fig. 4B), which can be induced by the ligand exchange with phosphate ions carrying excess negative charges probably changing the particle-cell interaction. It should be noted that the internalization of negatively charged iron oxide particles occurs via nonspecific binding to relatively scattered cationic sites present on the cell membrane and endocytosis [32]. This significantly limits interactions and can explain lower magnetically induced association of the γ-Fe_2O_3@PLL and γ-Fe_2O_3@PPLL particles with the cells than that of nanomag®-D. Enhanced amount of cell-associated nanomag®-D particles can be ascribed to their ability to form larger aggregates in magnetic field than PLL-coated magnetic nanoparticles do, increasing thus both the sedimentation rate and cellular uptake due to lower Brownian forces and higher pressure exerted on the cell membrane.

To determine whether PPLL might reduce cellular ROS levels, γ-Fe_2O_3@PLL and γ-Fe_2O_3@PPLL particles (100 μg/mL) were incubated with U87MG cells for 3 h, which was followed by staining with CM-H_2DCFDA for 1 h. Fig. 6 illustrates U87MG cellular uptake of γ-Fe_2O_3@PLL and γ-Fe_2O_3@PPLL particles and ROS levels. After the incubation with γ-Fe_2O_3@PLL and γ-Fe_2O_3@PPLL particles, SSC-H was dramatically up-shifted (Fig. 6B–G) compared to the control cells (Fig. 6A), suggesting an increase in cellular complexity and nanoparticle internalization. In addition, FSC-H was left-shifted compared to the control, suggesting reduction in size. These effects are in agreement with previous findings on cellular responses to nanoparticle internalization [7]. In addition, the cellular ROS signal was reduced to 54–64% (Fig. 6B–G) from a basal level of 77% (Fig. 6A). Summarized antioxidant activities of γ-Fe_2O_3@PLL and γ-Fe_2O_3@PPLL particles on three batches of U87MG cells indicated that application of these nanoparticles decreased the endogenous ROS level by 10–18% (Fig. 6H). The results suggest that γ-Fe_2O_3@PLL and γ-Fe_2O_3@PPLL nanoparticles are likely to be internalized by glioma cells, exerting antioxidant effect to reduce endogenous ROS at the cellular level. These particles were nontoxic and their antioxidative properties were much lower compared to those of free gallic acid. In fact, iron oxide nanoparticles are most likely to increase intracellular levels of ROS after internalization and degradation. Antioxidant characteristics of the γ-Fe_2O_3@PPLL particles can be thus very plausible in future applications (MRI, drug delivery systems) to reduce potential cytotoxicity associated with the iron oxide nanoparticles [33,34]. The antioxidant effect of PLL, as well as of other radical scavenging amino acids, is in agreement with previous findings that PLL-coated Fe_3O_4 nanoparticles could decrease the ROS level in cancer stem cells due to the interaction of terminal amino groups with

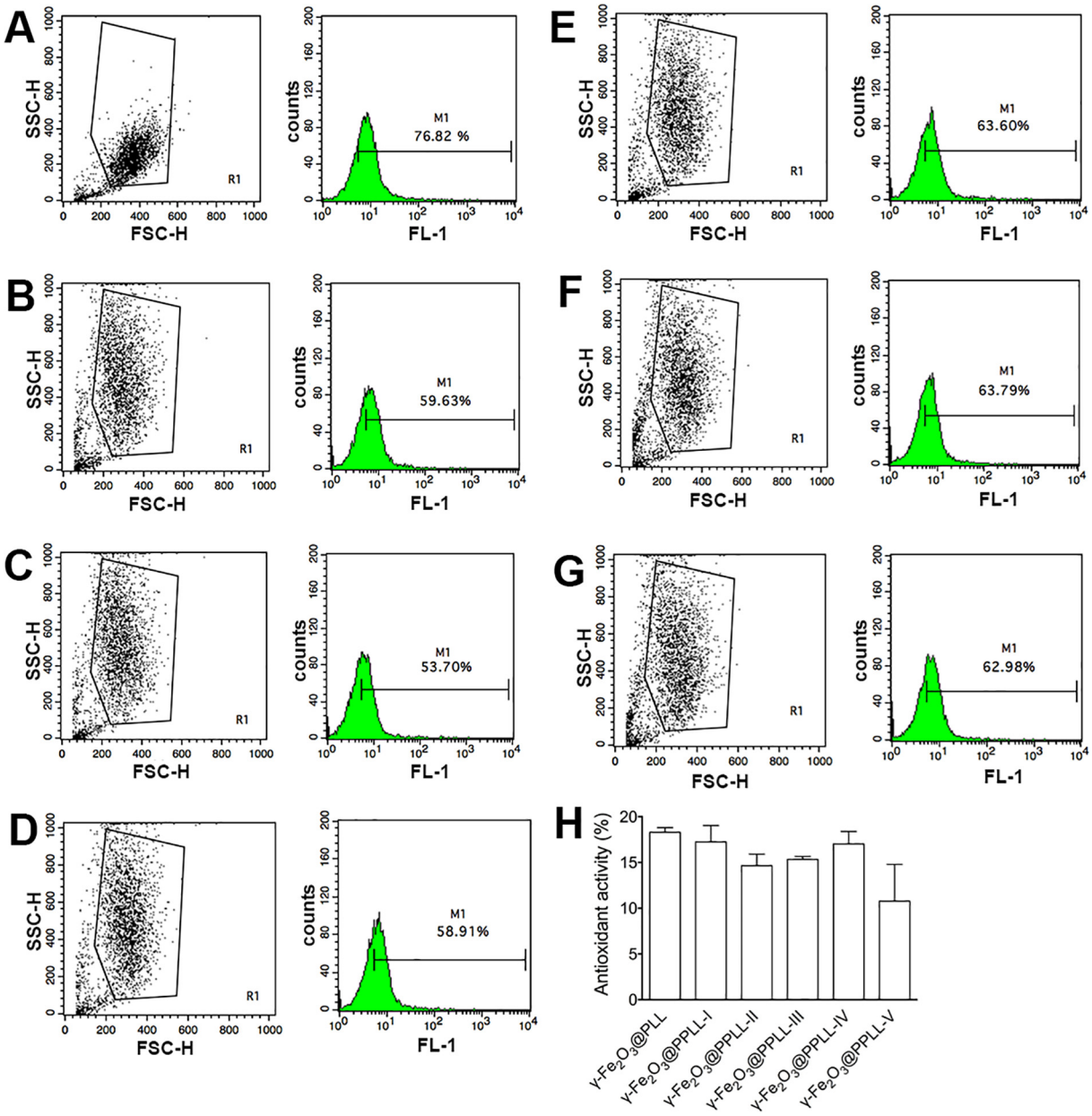

Fig. 6. Flow cytometry analysis of antioxidant activity of γ-Fe_2O_3@PLL and γ-Fe_2O_3@PPLL nanoparticles on cellular ROS levels. Endogenous ROS levels of U87MG cells in (A) absence and presence of 100 μg/mL of (B) γ-Fe_2O_3@PLL or (C-G) γ-Fe_2O_3@PPLL-I-V, respectively; incubation time 3 h. (H) Antioxidant activity of γ-Fe_2O_3@PLL and γ-Fe_2O_3@PPLL-I-V normalized to endogenous ROS level. Values are means ± SE (n = 3).

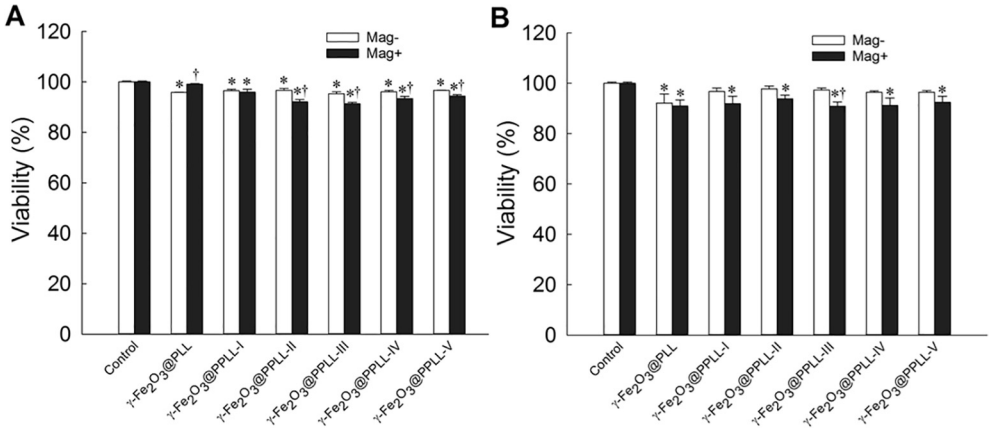

Fig. 7. Cytotoxicity of γ-Fe_2O_3@PLL and γ-Fe_2O_3@PPLL-I-V particles (100 μg/mL) with U87MG cells. Magnetic field was applied for 5 min before (Mag−) or during the incubation (Mag+) for (A) 3 and (B) 24 h. Values are means ± SE (n = 4). $^{*,\dagger}p < 0.05$ compared with the corresponding control and Mag-groups, respectively. Control was performed in the absence of the particles.

radicals [35–37]. Nevertheless, additional modification of the particles with the PPLL did not further enhance the ROS scavenging activity. Gallic acid- and poly(gallic acid)-coated Fe_3O_4 nanoparticles have been shown to exert antioxidant effects in A431 and Hela cells [38,39], suggesting an increase in the density of the phenolic groups on γ-Fe_2O_3@PLL may be required to further increase the antioxidant effects of γ-Fe_2O_3@PPLL. Moreover, the particles (100 μg/mL) induced very minor cytotoxicity after 3 or 24 h of incubation with the U87MG cells (Fig. 7), which is consistent with the toxicity observed in mensenchymal stem cells [16]. Enhanced internalization of the γ-Fe_2O_3@PLL and γ-Fe_2O_3@PPLL nanoparticles thus did not affect the cell viability.

4. Conclusion

Magnetic nanomaterials with antioxidant properties combine several advantages within the same particle. These include manipulability by magnetic field, easy magnetic separation from complex mixtures and redispersion in fluids when the magnet is removed, *in vitro* and *in vivo* detection by MRI, conjugation with biomolecules (drugs, peptides, nucleic acids, enzymes), and last but not least, prevention of cell damaging by elevated oxidative stress. In this report, γ-Fe_2O_3@SiO_2-PEI-PEG particles were prepared, which can withstand engulfment by the reticuloendothelial system. To render the γ-Fe_2O_3@SiO_2-PEI-PEG nanoparticles with antioxidant activity, PPLL containing several phenolic compounds was synthetized and used as an additional coating, which is biocompatible, chemically modifiable, and/or has transfection ability. PLL is a polyelectrolyte that can be adsorbed on the γ-Fe_2O_3@SiO_2 nanoparticle surface to maintain their colloidal stability in water by strong electrostatic repulsions. However, such a colloid could be unstable in biological media due to neutralization of the particle charge by counter ion layer formed in the presence of proteins and electrolytes, such as NaCl, KCl, Na_2HPO_4, and KH_2PO_4; therefore, presence of additional steric stabilizer (PEG) was required to prevent the particles from aggregation.

Antioxidant properties of the surface-modified iron oxide particles are usually characterized using chemical methods, typically 2,2-diphenyl-1-picrylhydrazyl (DPPH) assay [40]. In contrast, our report is focused on analyzing the antioxidant effects of the γ-Fe_2O_3@PLL and γ-Fe_2O_3@PPLL nanoparticles at the cellular level. The particles were found to be well internalized by glioma cells, twice as much as the nanomag®-D particles. However, the magnetic field increased internalization of the nanomag®-D, but not the γ-Fe_2O_3@PLL or γ-Fe_2O_3@PPLL particles. Cellular uptake is critical in future applications to target therapeutic agents to a diseased organ. Phenolic compounds bound to the particles did not affect their uptake by the cells or ROS scavenging ability of PLL. γ-Fe_2O_3@PLL itself showed significant antioxidant effect in glioma cells. According to the flow cytometry, both γ-Fe_2O_3@PLL and γ-Fe_2O_3@PPLL nanoparticles increased the antioxidant activity by almost 20% compared to EGCG-modified Fe_3O_4 used in previous report [7]. This reduction of the oxidative stress is significant in terms of combating serious diseases, such as cancer, atherosclerosis, myocardial infarction, or many neurodegenerative disorders.

Acknowledgements

This work was supported by the Czech Science Foundation (No. 16-01128J), Ministry of Science and Technology (Taiwan, 105-2923-B-182-001-MY3), and Chang Gung Memorial Hospital (BMRP432). We thank Core Instrument Center, Chang Gung University, Taoyuan, Taiwan, for assistance in the flow cytometry study.

Appendix A. Supplementary data

Supplementary data to this article can be found online at https://doi.org/10.1016/j.jmmm.2018.10.081.

References

[1] E.J. Ladas, J.S. Jacobson, D.D. Kennedy, K. Teel, A. Fleischauer, K.M. Kelly, Antioxidants and cancer therapy: a systematic review, J. Clin. Oncol. 22 (2004) 517–528.
[2] G. Bjelakovic, D. Nikolova, L.L. Gluud, R.G. Simonetti, C. Gluud, Mortality in randomized trials of antioxidant supplements for primary and secondary prevention. Systematic review and meta-analysis, J. Am. Med. Assoc. 297 (2007) 842–857.
[3] H. Numsen, M. Cortes, E.N. Drake, J.E. Spallholz, Cancer chemoprevention: a radical perspective, J. Free Radic. Biol. Med. 45 (2008) 97–110.
[4] C.S. Yang, P. Maliakal, X. Meng, Inhibition of carcinogenesis by tea, Annu. Rev. Pharmacol. Toxicol. 42 (2002) 25–54.
[5] Y.C. Hsu, Y.M. Liou, The anti-cancer effects of (−)-epigalocatechine-3-gallate on the signaling pathways associated with membrane receptors in MCF-7 cells, J. Cell. Physiol. 226 (2011) 2721–2730.
[6] C.S. Yang, X. Wang, G. Lu, S.C. Picinich, Cancer prevention by tea: animal studies, molecular mechanisms and human relevance, Nat. Rev. Cancer 9 (2009) 429–439.
[7] Y.-C. Lu, P.-C. Luo, C.-W. Huang, Y.-L. Leu, T.-H. Wang, K.-C. Wei, H.-E. Wang, Y.-H. Ma, Augmented cellular uptake of nanoparticles using tea catechins: effect of surface modification on nanoparticle-cell interaction, Nanoscale 6 (2014) 10297–10306.
[8] R.G. Chaudhuri, S. Paria, Core/shell nanoparticles: classes, properties, synthesis mechanisms, characterization, and applications, Chem. Rev. 112 (2012) 2373–2433.
[9] A.-H. Lu, E.L. Salabas, F. Schuth, Magnetic nanoparticles: synthesis, protection, functionalization, and application, Angew. Chem. Int. Ed. 46 (2007) 1222–1244.
[10] I.F. Cheng, K. Breen, On the ability of four flavonoids, baicilein, luteolin, naringenin, and quercetin, to suppress the Fenton reaction of the iron-ATP complex, Biometals 13 (2000) 77–83.
[11] M. Lurdes, M.T. Fernandez, M. Santos, R. Rocha, M.H. Florencio, K.R. Jennings, Interactions of flavonoids with iron and copper ions: a mechanism for their antioxidant activity, Free Radic. Res. 36 (2002) 1199–1208.
[12] D. Horák, M. Babič, P. Jendelová, V. Herynek, M. Trchová, Z. Pientka, E. Pollert, M. Hájek, E. Syková, D-mannose-modified iron oxide nanoparticles for stem cell labeling, Bioconjugate Chem. 18 (2007) 635–644.
[13] M. Babič, D. Horák, P. Jendelová, K. Glogarová, V. Herynek, M. Trchová, K. Likavčanová, M. Hájek, E. Syková, Poly(*N,* N-dimethylacrylamide)-coated maghemite nanoparticles for stem cell labeling, Bioconjugate Chem. 20 (2009) 283–294.
[14] Y.K. Buchman, E. Lellouche, S. Zigdon, M. Bechor, S. Michaeli, J.-P. Lellouche, Silica nanoparticles and polyethyleneimine (PEI)-mediated functionalization: a new method of PEI covalent attachment for siRNA delivery applications, Bioconjugate Chem. 24 (2013) 2076–2087.
[15] S. Laurent, D. Forge, M. Port, A. Roch, C. Robic, L.V. Elst, R.N. Muller, Magnetic iron oxide nanoparticles: synthesis, stabilization, vectorization, physicochemical characterizations, and biological applications, Chem. Rev. 108 (2008) 2064–2110.
[16] M. Babič, D. Horák, M. Trchová, P. Jendelová, K. Glogarová, P. Lesný, V. Herynek, M. Hájek, E. Syková, Poly(L-lysine)-modified iron oxide nanoparticles for stem cell labeling, Bioconjugate Chem. 19 (2008) 740–750.
[17] W.X. Siow, Y.T. Chang, M. Babič, Y.C. Lu, D. Horák, Y.H. Ma, Interaction of poly-L-lysine coating and heparan sulfate proteoglycan on magnetic nanoparticle uptake by tumor cells, Int. J. Nanomed. 13 (2018) 1693–1706.
[18] D. Mazia, G. Schatten, W. Sale, Adhesion of cells to surfaces coated with polylysine. Applications to electron microscopy, J. Cell Biol. 66 (1975) 198–200.
[19] X. Kong, L.C.L. Huang, S.C.V. Liau, C.C. Han, H.C. Chang, Polylysine-coated diamond nanocrystals for MALDI-TOF mass analysis of DNA oligonucleotides, Anal. Chem. 77 (2005) 4273–4277.
[20] B.L. Frey, C.E. Jordan, S. Kornguth, R.M. Corn, Control of the specific adsorption of proteins onto gold surfaces with poly(L-lysine) monolayers, Anal. Chem. 67 (1995) 4452–4457.
[21] S.I. Suye, Y. Kumon, A. Ishigaki, Immobilization of glucose oxidase on poly-(L-lysine)-modified polycarbonate membrane, Biotechnol. Appl. Biochem. 27 (1998) 245–248.
[22] M.W. Jones, G. Mantovani, C.A. Blindauer, S.M. Ryan, X. Wang, D.J. Brayden, D.M. Haddleton, Direct peptide bioconjugation/PEGylation at tyrosine with linear and branched polymeric diazonium salts, J. Am. Chem. Soc. 134 (2012) 7406–7413.
[23] A.M. Almeida, T.L. Andersen, A.T. Lindhardt, M.V. Almeida, T. Skrydstrup, General method for the preparation of active esters by palladium-catalyzed alkoxycarbonylation of aryl bromides, J. Org. Chem. 80 (2015) 1920–1928.
[24] V. Patsula, M. Moskvin, S. Dutz, D. Horák, Size-dependent magnetic properties of iron oxide nanoparticles, J. Phys. Chem. Solids 88 (2016) 24–30.
[25] Y.C. Lu, F.Y. Chang, S.J. Tu, J.P. Chen, Y.H. Ma, Cellular uptake of magnetite nanoparticles enhanced by NdFeB magnets in staggered arrangement, J. Magn. Magn. Mater. 427 (2017) 71–80.
[26] R.W. Hemingway, J.J. Karchesy, S.J. Branham (Eds.), Chemistry and Significance of Condensed Tannins, Plenum Press, New York, 1989.
[27] U.K. Das, J. Bobak, C. Fowler, S.E. Hann, C.F. Petten, L.N. Dawe, A. Decken, F.M. Kerton, C.M. Kozak, Synthesis and structure of mono-, bi- and trimetallic amine-bis(phenolate) cobalt(II) complexes, Dalton Trans. 39 (2010) 5462–5477.
[28] D.H. Everett, Why are colloidal dispersions stable? II. Interparticle forces, Basic Principles of Colloid Science, Royal Society of Chemistry, London, 1988, pp. 42–44.
[29] H.M. Eckenrode, H.L. Dai, Nonlinear optical probe of biopolymer adsorption on colloidal particle surface: poly-L-lysine on polystyrene sulfate microspheres, Langmuir 20 (2004) 9202–9209.

[30] C. Plank, F. Scherer, U. Schillinger, C. Bergemann, M. Anton, Magnetofection: enhancing and targeting gene delivery with superparamagnetic nanoparticles and magnetic fields, J. Liposome Res. 13 (2003) 29–32.
[31] S. Krishnan, C.J. Weinman, C.K. Ober, Advances in polymers for anti-biofouling surfaces, J. Mater. Chem. 18 (2008) 3405–3413.
[32] A. Verma, F. Stellacci, Effect of surface properties on nanoparticle–cell interactions, Small 6 (2010) 12–21.
[33] S.M. Hussain, K.L. Hess, J.M. Gearhart, K.T. Geiss, J.J. Schlager, In vitro toxicity of nanoparticles in BRL 3A rat liver cells, Toxicol. Vitro 19 (2005) 975–983.
[34] M. Calero, L. Gutiérrez, G. Salas, Y. Luengo, A. Lázaro, P. Acedo, M.P. Morales, R. Miranda, A. Villanueva, Efficient and safe internalization of magnetic iron oxide nanoparticles: two fundamental requirements for biomedical applications, Nanomedicine 10 (2014) 733–743.
[35] X. Wang, Q. Tu, B. Zhao, Y. An, J.C. Wang, W. Liu, M.S. Yuan, S.M. Ahmed, J. Xu, R. Liu, Y. Zhang, J. Wang, Effects of poly(L-lysine)-modified Fe_3O_4 nanoparticles on endogenous reactive oxygen species in cancer stem cells, Biomaterials 34 (2013) 1155–1169.
[36] S. Wallner, A. Hermetter, B. Mayer, T.C. Wascher, The alpha-amino group of L-arginine mediates its antioxidant effect, Eur. J. Clin. Invest. 31 (2001) 98–102.
[37] E.R. Stadtman, R.L. Levine, Free radical-mediated oxidation of free amino acids and amino acid residues in proteins, Amino Acids 25 (2003) 207–218.
[38] E. Tombácz, M. Szekeres, A. Hajdú, I. Tóth, R.A. Bauer, D. Nesztor, E. Illés, I. Zupkó, L. Vékás, Colloidal stability of carboxylated iron oxide nanomagnets for biomedical use, period, Polytech. Chem. Eng. 58 (2014) 3–10.
[39] M. Szekeres, E. Illés, C. Janko, K. Farkas, I.Y. Tóth, D. Nesztor, I. Zupkó, I. Földesi, C. Alexiou, E. Tombácz, Hemocompatibility and biomedical potential of poly(gallic acid) coated iron oxide nanoparticles for theranostic use, J. Nanomed. Nanotechnol. 6 (2015) 1000252.
[40] S.T. Shah, W.A. Yehye, O. Saad, K. Simarani, Z.Z. Chowdhury, A.A. Alhadi, L.A. Al-Ani, Surface functionalization of iron oxide nanoparticles with gallic acid as potential antioxidant and antimicrobial agents, Nanomaterials 7 (2007) 306.